Drag Perturbations of Near-Circular Orbits in an Oblate Diurnal Atmosphere

F. A. Santora*
General Electric Company, Valley Forge, Pa.

An improved theory is developed specifically for orbits of very small eccentricity ($e=0$ to 0.01). Analytic expressions are derived which describe perturbation rates in orbit period, eccentricity, and perigee argument. The equations include the combined effects of earth flattening, oblate earth mass, and the diurnal bulge. Singularities and ambiguities encountered with existing theory are removed by employing mean orbital elements. Comparisons of analytical averaging with numerical integration methods demonstrate intrinsic perturbation accuracies to within 2%, with an accomplished improvement of two orders of magnitude in computation time.

Introduction

PREVIOUSLY, the effect of drag perturbation on artificial satellites of very small eccentricity was studied by Cook, King-Hele,[1,2] Zee,[3] and others.[4,5] Generally, the available theories treat the effects of the earth's flattening or oblate earth figure, oblate earth mass, and diurnal atmosphere bulge separately. With the renewed interest[6-8] in satellite operational control by rapid and accurate prediction techniques, additional studies of drag decay theory become timely. Recently,[9] the effects of an oblate earth figure and diurnal bulge were combined, and gravitational perturbations caused by the oblate earth mass were accounted for by the use of a geometric perturbed orbit shape. However, theories to date still suffer considerably in accuracy when very small orbit eccentricities ($e\approx 0$) are encountered. Inaccuracies stem from the following two facts not considered previously. First, short term gravitational perturbations cause the orbital flight path to be far different than that predicted by classic orbit elements. This flight path departure actually may produce two perigees and two apogees during a single orbit revolution, thereby leading to ambiguities and erroneous use of the developed theories. Second, the density profiles associated with such flight path departures are not accommodated by available theories, thus leading to further inaccurate prediction of drag perturbations. This paper derives a new theory developed especially for orbits of very small eccentricity ($e=0$ to 0.01). The derived theory also is "unified" in that it includes both the effects of an oblate earth figure, short and long term gravitational perturbations, and the effects of a diurnal bulge. With realistic perturbation expressions available, both drag and gravitational perturbations can be estimated quickly and summed to obtain reasonable decay histories without numerical integration.

Approach

Figure 1 depicts the assumed physical model of the oblate earth figure and atmosphere bulge, which has a declination of δ_B. For purposes of illustration, the actual flight path of a polar orbit also is shown. Note the possibility of four apses along the true path. Also shown is the corresponding mean orbit path, which excludes gravitational perturbations. The perigee argument of the mean orbit is given by $\bar{\omega}$, and is located at an angular distance ϕ from the bulge center. Similar to previous work,[1,2,9] a constant altitude surface is established at a radius distance of r_o. Unlike previous work, the constant altitude is not the osculating perigee value, but rather is the osculating altitude of the actual orbit corresponding to the $\bar{\omega}$ location (i.e, $\lambda=\bar{\omega}$). It is further assumed[1,9] that the maximum density ρ_{max} on the constant altitude surface is at the bulge center, and the minimum density point ρ_{min} is diametrically opposite the bulge center. The approach taken is to determine the air density ρ along the perturbed path r, but apply this actual encountered density to the mean orbit path, $\bar{r}$. In other words, the satellite mathematically orbits in the mean orbit but experiences the drag deceleration of its real orbital path. In this way, realistic perturbations in the mean orbital elements are obtained. Appropriate conversions then can be made to find the actual or osculating orbit conditions.

Air Density

The geocentric radius σ of the constant altitude surface in Fig. 1 was derived previously[2] and is repeated here

$$\sigma=r_o[1-1/2\epsilon\sin^2 i\cos 2\bar{\omega}+1/2\epsilon\sin^2 i\cos 2\lambda] \tag{1}$$

where ϵ is Earth's flattening constant, i is the orbit inclination, and r_o is the osculating radius at $\lambda=\bar{\omega}$. The argument of spacecraft position is λ. Taking an identical approach to that of Cook and King-Hele,[1,10] the density ρ along the actual or perturbed orbit path is expressed as a sinusoidal variation on the constant altitude surface and adjusted exponentially for the $r-\sigma$ difference

$$\begin{aligned}\rho&=\rho_o[1+F\cos\phi]\exp\{-\beta(r-\sigma)\}\\&=\rho_o[1+FA\cos(\bar{\omega}-\lambda)-FB\sin(\bar{\omega}-\lambda)]\exp\\&\{-\beta(r-r_o)-c\cos\bar{\omega}+c\cos 2\lambda\}\end{aligned} \tag{2}$$

In Eq. (2), ρ_o is the average density on the constant altitude surface, F is the density amplitude factor, and β is the inverse of the density scale height ($\beta=1/H$), which can be determined in a manner described in Ref. 9. With orbits of very small eccentricity, H is simply the average evaluated on the constant altitude surface. A and B are modulation coefficients dependent on the orbit orientation relative to the bulge center. In Eqs. (3-7), the right ascension of the bulge center is specified by β_B, and the right ascension of the orbit by Ω

$$\rho_o=1/2\ (\rho_{max}+\rho_{min}) \tag{3}$$

$$F=(\rho_{max}-\rho_{min})\ /\ (\rho_{max}+\rho_{min}) \tag{4}$$

Presented as Paper AAS 75-025 at the AAS/AIAA Astrodynamics Specialist Conference, Nassau, Bahamas, July 28-30, 1975; submitted Sept. 19, 1975; revision received April 13, 1976.
Index category: Earth-Orbital Trajectories.
*Systems Engineer. Member AIAA.

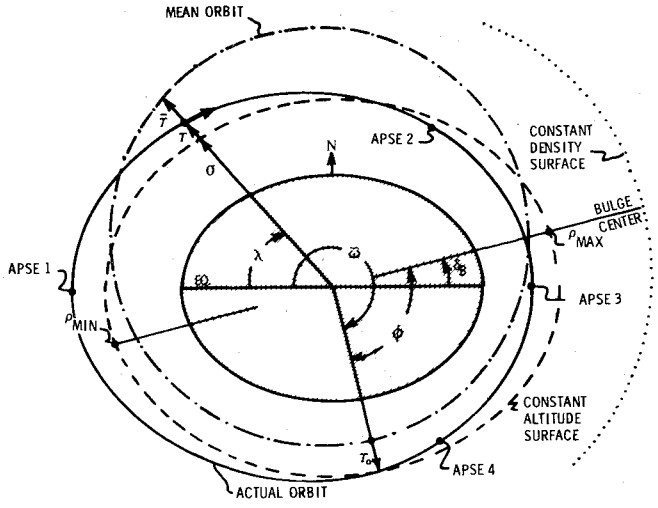

Fig. 1 Geometric description.

$$A=\sin\delta_B \sin i \sin\bar{\omega}+\cos\delta_B[\cos(\Omega-\alpha_B)\cos\bar{\omega} - \cos i \sin(\Omega-\alpha_B)\sin\bar{\omega}] \quad (5)$$

$$B=\sin\delta_B \sin i \cos\bar{\omega}-\cos\delta_B[\cos(\Omega-\alpha_B)\sin\bar{\omega} + \cos i \sin(\Omega-\alpha_B)\cos\bar{\omega}] \quad (6)$$

$$c=1/2\beta r_o \epsilon \sin^2 i \quad (7)$$

In order to express Eq. (2) entirely in terms of mean orbital elements, which are required for integration purposes, it first becomes necessary to examine gravitationally induced perturbations on the orbit path.

Gravitational Perturbations

Usually the osculating or instantaneous state (a, e, i, ω, Ω, θ) of a satellite is either known or initially assumed. The true anomaly of the satellite is denoted by θ, and the argument of position is given by $\lambda=\omega+\theta$. The orbit semimajor axis is a. From Kozai,[11] the following constants can be written

$$C=(A_2/a^2)\ (1-3/2\sin^2 i) \quad (8)$$

$$D=(A_2/a^2)\sin^2 i \quad (9)$$

$$E=\left[3/4(A_3/A_2)a^{-1}-15/16(A_5/A_2)a^{-3}F(i) - 105/512(A_7/A_2)a^{-5}F'(i)\right]\sin i \quad (10)$$

In Eqs. (8-10), A_2, A_3, A_5, and A_7 are the Kozai[12]-defined harmonic coefficients of the potential function. Also, from Refs. 11 and 13, $F(i)$ and $F'(i)$ are defined as

$$F(i)=(8-28\sin^2 i+21\sin^4 i)/(4-5\sin^2 i) \quad (11)$$

$$F'(i)=(64-432\sin^2 i+792\sin^4 i-429\sin^6 i)/(4-5\sin^2 i) \quad (12)$$

Again from Kozai,[12] the mean orbital elements can be found by assuming that the true anomaly is equal to the mean anomaly for orbits of very small eccentricity. The mean semimajor axis $\bar{a}$ is simply

$$\bar{a}=a\ (1-D\cos 2\lambda) \quad (13)$$

and the mean orbit eccentricity

$$\bar{e}=[e_o^2+C^2+29/72D^2+E^2]^{1/2} \quad (14)$$

In Eq. (14), e_o is the proper eccentricity[12] or the orbit eccentricity that would be realized for a spherically symmetric Earth mass. It is important to note that $\bar{e}$ and e_o always retain a positive value greater than zero, which eliminates singularities normally associated with orbit perturbation equations when $e=0$. In terms of the osculating state, it can be shown that e_o is given by

$$e_o=[e^2+C^2+29/72\,D^2+E^2+5/3CD\cos 2\lambda + 7/24D^2\cos 4\lambda-2eC\cos(\omega-\lambda)-1/2e\,D\cos(\omega+\lambda) - 7/6\,eD\cos(\omega-3\lambda)-2e\,E\sin\omega+1/2\,E(4C-D)\sin\lambda + 7/6\,DE\sin 3\lambda]^{1/2} \quad (15)$$

The mean perigee argument $\bar{\omega}$ also can be found from Kozai[12]

$$\bar{\omega}=\tan^{-1}[(e_o\sin\bar{\omega})\ /\ (e_o\cos\bar{\omega})] \quad (16)$$

where

$$e_o\sin\bar{\omega}=e\sin\omega-(C-1/4D)\sin\lambda-7/12\,D\sin 3\lambda-E \quad (17)$$

and

$$e_o\cos\bar{\omega}=e\cos\omega-(C+1/4\,D)\cos\lambda-7/12\,D\cos 3\lambda \quad (18)$$

Following Kozai's method, and after some manipulation and elimination of second-order and higher terms, the actual orbital radius can be written in terms of the mean orbit. Although the mean eccentricity does not appear explicitly in Eq. (19), it is however, from Eq. (14), inherent in e_o. Essentially, Eq. (19) gives the osculating radius in terms of a pseudomean orbit expressed by $\bar{a}$, $\bar{\omega}$, and e_o. This equation generally is accurate to within 0.05 n mi (0.1 km)

$$r=\bar{a}[1-e_o\cos(\bar{\omega}-\lambda)-C+1/6\,D\cos 2\lambda-E\sin\lambda] \quad (19)$$

The radius r_o used to establish the constant altitude surface now can be obtained from Eq. (19) simply by substituting $\lambda=\bar{\omega}$.

When the mean elements are known, the corresponding osculating value of semimajor axis for a given value of λ can be solved from Eq. (13). However, the osculating values of eccentricity e and perigee argument ω must be determined with the use of Eqs. (20) and (21):[12]

$$e\cos\omega=e_o\cos\bar{\omega}+(C+1/4\,D)\cos\lambda+7/12\,D\cos 3\lambda \quad (20)$$

$$e\sin\omega=e_o\sin\bar{\omega}+(C-1/4\,D)\sin\lambda+7/12\,D\sin 3\lambda+E \quad (21)$$

Therefore

$$e=[(e\sin\omega)^2+(e\cos\omega)^2]^{1/2} \quad (22)$$

and $\omega=\tan^{-1}(\sin\omega/\cos\omega)$. Equations reflect the perturbations in a (7,0) geopotential field; i.e, the potential in expanded spherical harmonics up to the seventh cosine harmonic coefficient, and without any sine harmonic coefficients.

It is pointed out that $\bar{\omega}$ precesses monotonically, at its usual secular rate $\dot{\bar{\omega}}$, even though ω may oscillate about some constant value[12] in the case of very small eccentricities. Furthermore, for small eccentricities, there are only two apses associated with the mean orbit, rather than possibly four, as deduced from Eq. (19). Thus, use of the mean orbit eliminates ambiguities in specifying and predicting apses; and because of its conventional characteristics and behavior, drag perturbation equations can be applied directly.

Drag Perturbations

General drag perturbation equations have been derived previously[1,2] in terms of the eccentric anomaly. By transforming the equations into a form containing true anomaly θ under a small eccentricity assumption, the expressions can be converted further by $\theta=\lambda+\bar{\omega}$ to those shown by Eqs. (23–25). Since r in Eq. (19) is expressed by the elements of $\bar{a}$, $\bar{\omega}$, and $e_o=f(\bar{e})$, it is easier to formulate the perturbation equations using e_o rather than $\bar{e}$. The perturbations over one orbit revolution due to drag of the mean semimajor axis $\Delta\bar{a}$, the eccentricity parameter $\Delta(\bar{a}\,e_o)$, and the perigee argument $\Delta\bar{\omega}$ are, respectively

$$\Delta\bar{a}=-\delta\bar{a}^2\int_{\lambda=o}^{2\pi}\rho[1+e_o\cos(\bar{\omega}-\lambda)]\,d\lambda \tag{23}$$

$$\Delta(\bar{a}\,e_o)=-\delta\bar{a}^2\int_{\lambda=o}^{2\pi}\rho[3/2e_o+\cos(\bar{\omega}-\lambda) -1/2e_o\cos2(\bar{\omega}-\lambda)]\,d\lambda \tag{24}$$

$$\Delta\bar{\omega}=-\delta\left(\frac{\bar{a}}{e_o}\right)\int_{\lambda=o}^{2\pi}\rho\Big[\sin(\lambda-\bar{\omega}) -1/2e_o\sin^2(\lambda-\bar{\omega})\,d\lambda \tag{25}$$

By substituting r_o derived from Eq. (19) into Eq. (2), the general expression for air density to be used in Eqs. (23-25) can be obtained

$$\rho=\rho_o[1+FA\cos(\bar{\omega}-\lambda)-FB\sin(\bar{\omega}-\lambda)]\exp\{-z_o/\cos\bar{\omega}+(z_1-c)\cos2\bar{\omega} -z_3\sin\bar{\omega}\}\exp\{z_o\cos\lambda+z_2\cos2\lambda+z_4\sin\lambda\} \tag{26}$$

where the constants are defined as

$$z_o=\beta\bar{a}\,e_o\cos\bar{\omega} \tag{27}$$

$$z_1=1/6\beta\bar{a}D \tag{28}$$

$$z_2=c-z_1 \tag{29}$$

$$z_3=\beta\bar{a}E \tag{30}$$

$$z_4=\beta\bar{a}(E+e_o\sin\bar{\omega}) \tag{31}$$

Representing the exponential terms of Eq. (26) as

$$EX_1=\exp\{-z_o/\cos\bar{\omega}-z_2\cos2\bar{\omega}-z_3\sin\bar{\omega}\} \tag{32}$$

$$EX_2=\exp\{z_2\cos2\lambda+z_4\sin\lambda\} \cong 1+z_2\cos2\lambda z_4\sin\lambda+1/2z_4\sin^2\lambda \tag{33}$$

Eqs. (23–25) can be rewritten

$$\Delta\bar{a}=-\delta\bar{a}^2\rho_oEX_1\int_o^{2\pi}EX_2[1 +FA\cos(\bar{\omega}-\lambda)-FB\sin(\bar{\omega}-\lambda)]\cdot[1+e_o\cos(\bar{\omega} -\lambda)]\cdot\exp\{z_o\cos\lambda\}\,d\lambda \tag{34}$$

$$\Delta(\bar{a}\,e_o)=\delta\bar{a}^2\rho_o\,EX_1\int_0^{2\pi}EX_2[1+FA\cos(\bar{\omega} -\lambda)-FB\sin(\bar{\omega}-\lambda)]\cdot[3/2e_o+\cos(\bar{\omega}-\lambda) -1/2e_o\cos2(\bar{\omega}-\lambda)]\exp\{z_o\cos\lambda\}\,d\lambda \tag{35}$$

$$\Delta\bar{\omega}=-\delta\left(\frac{a}{e_o}\right)\rho_oEX_1\int_o^{2\pi}EX_2[1+FA\cos(\bar{\omega} -\lambda)-FB\sin(\bar{\omega}-\lambda)]\cdot[\sin(\lambda-\bar{\omega})-1/2\,e_o\sin2(\lambda-\bar{\omega})] \exp\{z_o\cos\lambda\}\,d\lambda \tag{36}$$

δ in Eqs. (34–36), is a constant that included the satellite ballistic coefficient (C_DA_{REF}/m) and a correction factor for atmosphere rotation

$$\delta=(C_DA_{REF}/m)[1-(r_o/v_o)\,\Lambda\omega_E\cos i]^2 \tag{37}$$

Λ is the ratio of the atmosphere angular rotation to the earth rotation, ω_E; and v_o is the satellite speed at r_o.

Equations (34–36) are manipulated to achieve integrable representations of Bessel functions of the first kind and imaginary argument of the form $I_n(z_o)$

$$I_n(z_o)=\frac{1}{2\pi}\int_o^{2\pi}\cos n\lambda\exp\{z_o\cos\lambda\}\,d\lambda \tag{38}$$

The analytical solutions of Eqs. (34–36) for very small eccentricities over one orbit revolution are given by the simple expressions that follow. The effects of Earth's flattening (contained in EX_1), atmosphere bulge (FA and FB), and perturbed flight path (z_1's) are easily discernible

$$\Delta\bar{a}=-2\pi\delta\bar{a}^2\rho_oEX_1\{I_o+z_2I_2+1/4z_4^2(I_o-I_2)+1/2e_oFA\,I_o+[1/2z_4FB(I_o-I_2)+FA(1+1/2z_2+1/8z_4^2)I_1]\cos\bar{\omega} +[1/2z_4FA(I_o-I_2)-FB(1+1/2z_2+1/8z_4^2)I_1]\sin\bar{\omega}\} \tag{39}$$

$$\Delta(\bar{a}\,e_o)=-\pi\delta\bar{a}^2\rho_oEX_1\{FA[(1+1/4z_4^2)I_o+z_2I_2]+3/2\,e_oI_o+2(1+1/2z_2+1/8z_4^2)I_1\cos\bar{\omega}+z_4(I_o-I_2)\sin\bar{\omega}+\{1/2z_4FBI_1+FA[I_2+1/2z_2I_o-1/8z_4^2(I_o-2I_2)]\}\cos2\bar{\omega} +\{1/2z_4FA\,I_1-FB[I_2+1/2z_2I_o-1/8z_4^2(I_o-2I_2)]\}\sin2\bar{\omega}\} \tag{40}$$

$$\Delta\bar{\omega}=-\pi\delta(\bar{a}/e_o)\rho_oEX_1\{FB[(1+1/4z_4^2)I_o+z_2I_2]-2(1+1/2z_2+1/8z_4^2)I_1\sin\bar{\omega}+z_4(I_o-I_2)\cos\bar{\omega} -\{1/2z_4I_1FB+FA[I_2+1/2z_2I_o-1/8z_4^2(I_o-2I_2)]\}\sin2\bar{\omega}+\{1/2z_4I_1FA-FB[I_2+1/2z_2I_o-1/8z_4^2(I_o-2I_2)]\}\cos2\bar{\omega}\Big\} \tag{41}$$

The change in the proper orbit eccentricity is found from

$$\Delta e_o=[\Delta(\bar{a}\,e_o)-e_o\Delta\bar{a}]/\bar{a} \tag{42}$$

and the corresponding change in the mean orbit eccentricity is

$$\Delta\bar{e}=(e_o/\bar{e})\Delta e_o \tag{43}$$

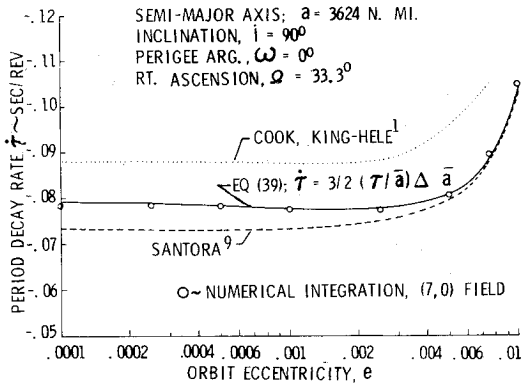

Fig. 2 Orbit period decay rate comparison.

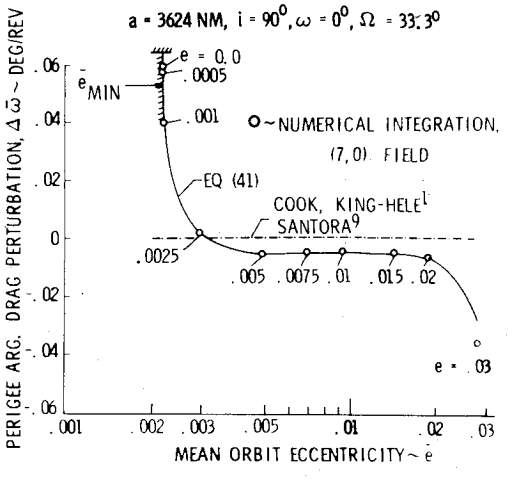

Fig. 3 Minimum mean eccentricity.

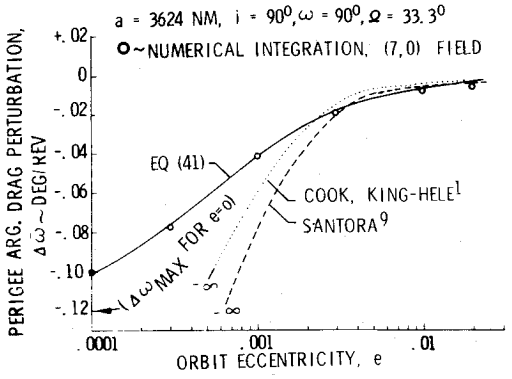

Fig. 4 Perigee argument perturbation comparison.

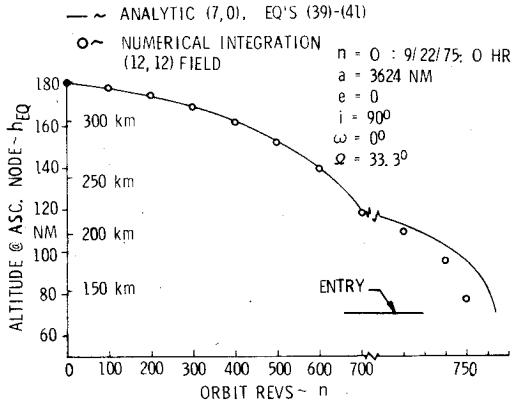

Fig. 5 Altitude decay history.

Numerical Results

The drag perturbation equations (Eqs. 23-43) were evaluated by use of a Walker modified Jacchia '67 atmosphere[14] for several sample cases. Atmospheric conditions consisted of a mean solar flux value of $FL=150\cdot10^{-22}$ W/m^2/cps, and a geomagnetic activity index $a_p=20$ ($2\cdot10^{-5}$G). The data selected for density computations is 0 hr, Sept. 22, 1975; which places the sun at the atumnal equinox. A ballistic coefficient of $C_DA_{REF}/m=2.0$ ft^2/slug (0.0137m^2/kg) is arbitrairily selected for all cases, and the atmosphere rotation parameter Λ is taken as unity. Figure 2 presents a comparison of nodal period decay rates ($\dot{t}$) as computed by various theories. The data represent that of a polar orbit having a right ascension of $\Omega=33.3°$, which places the orbit plane in the center of the bulge. The osculating element values are $a=3624$ nautical mile (6711.65 km), with $\omega=0°$ with eccentricity varying from $e=0.0001$-0.01. Also included in Fig. 2 are sample results of numerical integration in a (7,0) field. It can be seen that available theories can result in decay rate errors of 8–15% in this small eccentricity range, whereas, the results computed by Eq. (39) are in a very close agreement (<2% error) with the numerically integrated data.

Figure 3 shows a similar comparison in the perigee argument perturbation rate ($\Delta\bar{\omega}$) for the same conditions. Note first of all that the available theories show zero perturbations in perigee argument. This case was selected purposely with $\omega=0$ so as to place the osculating perigee at the bulge center, which in turn is located in the equatorial plane. Since available theories assume an unperturbed elliptical path, and as a result of the selected conditions, the drag deceleration experienced between apses will be balanced. Thus, the consequence is a zero perturbation rate ($\Delta\bar{\omega}=0$), regardless of the eccentricity value. However, this zero perturbation rate is not true, as is evidenced by the results of numerical integration. Actually the gravitationally perturbed flight path results in a mean orbit whose perigee is displaced from the equatorial plane and whose osculating altitude history is not symmetrical about the line of apsides. The ability of Eq. (41) to simulate these complications and provide a correct perturbation rate also is evident, even for the case of an osculating eccentricity value equal to zero ($e=0$). It is important also to note that the mean eccentricity reaches some minimum value greater than zero, in this case, $\bar{e}_{min}\approx0.0024$. The corresponding value of e_o is generally about one-half of $\bar{e}$, thereby preventing any singularities in $\Delta\bar{\omega}$ from occuring. For this reason, it is not neccessary to transform the perturbation equations by a substitution of variables as was done by Cook and King-Hele[1] for the case of high-drag deceleration.

Figure 4 shows another comparison of perigee argument perturbations for the same conditions as the preceding, except that the osculating perigee argument is $\omega=90°$. This condition results in non-equal density flight profiles between apses, thereby generating perturbations in the mean perigee argument $\bar{\omega}$. The figure shows good agreement with other theories for eccentricities greater than about 0.01, but becomes increasingly large in error as the singularity ($e=0$) is approached. Equation (41) shows almost perfect agreement with numerical integration results for eccentricities less than 0.01, but slightly increasing in error for higher eccentricities. Again, because $\bar{e}$ and e_o do not attain a zero value, accuracy is retained even in the neighborhood of $e=0$.

Figure 5 presents an altitude decay history prediction for an orbit having an approximate 45-day lifetime. The initial conditions of the orbit are as noted, and are equivalent to an approximate 180-n mi (333.36-km) circular orbit at the equator. The analytic history in Fig. 5 was obtained by a numerical averaging technique in which the mean elements were updated with the algebraic addition of their perturbations on a revolution-by-revolution basis. The osculating state then was

obtained from the updated mean elements by use of the ancillary (Eqs. (13–22). Entry, as predicted by Eqs. (39–41) occurs less than 15 revolutions after that computed by numerical integration using a (12,12) geopotential field. The divergence between the analytic solution and the integration results near entry is attributed to large altitude perturbations greater than 0.5 nautical miles (1 km), which are beyond the capability of the non-iterative use of the perturbation equations. Computational time to integrate the orbit in a (12,12) field for 750 revolutions can require up to three hours, depending on the specific computer and program; whereas, the same orbit history could be generated in less than a minute with the analytical averaging approach.

Concluding Remarks

The major contribution of this paper is the presentation of a new "unified" theory that provides a high degree of drag perturbation prediction accuracy for near-circular orbits ($e=0$ to 0.01). Typical results show intrinsic accuracies to within 2% when using a Walker modified Jachia 1967 atmosphere model. The derived perturbation equations include the combined effects of gravitational perturbations on orbit flight path, earth's flattening on altitude, and the diurnal bulge on day-to-night density variation. Most significantly the perigee argument perturbation can be predicted to less than 5% error, rather than a 30% or greater errors. This is extremely important since the cumulative effect of any error over hundreds of revolutions can lead to serious error in the predicted decay history. Thus, in operational flight, additional errors will be a result only of atmosphere model and ballistic coefficient uncertainties. Because of its accuracy and computational speed, the theory is useful as either a design tool for lifetime time prediction and mission analyses, or as a means for in-flight monitoring and control of operational satellites. Finally, the theory also can be used in its inverse form to solve for the "effective" ballistic coefficient when given an observed decay rate; and to isolate certain atmospheric and earth dynamical parameters.

References

[1]Cook, G. E., and King-Hele, D. G., "The Contraction of Satellite Orbits under the Influence of Air Drag, Part VI: Near-Circular Orbits with Day-to-Night Variation in Air Density," Royal Aircraft Establishment, Tech. Rept. RAF 67092, April 1967.

[2]Cook, G. E., and King-Hele, D. G., and Walker, D., "The Contraction of Satellite Orbits under the Influence of Air Drag, Part II: with Oblate Atmosphere," *Proceedings of the Royal Society,* Vol. 264, 1961.

[3]Zee, C. H. "Trajectories of Satellites under the Combined Influences of Earth Oblateness and Air Drag," *Celestial Mechanics,* Vol. 3, 1971, pp. 148–168.

[4]Lane, M. H., "The Development of an Artificial Satellite Theory Using a Power-Law Atmospheric Density Representation," AIAA Paper 65-35, Jan. 1965

[5]Otterman, J., and Lichtenfeld, K., "Effects of Air Drag on Near-Circular Satellite Orbits," *Journal of Spacecrafts and Rockets,* Vol. 5, Sept. 1964, pp. 513–519.

[6]Wexler, D. M. "Rapid Orbit Prediction Program ("ROPP"),," prepared for A. F. Cambridge Research Lab. by TRW Systems, Contract No. F19628-68-C-0170, Rept. 09967-6001-R0-00, Oct. 1968.

[7]Velez, C. E. and Fuchs, A. J., "Averaging Techniques and Their Application to Orbit Determination Systems," *AIAA Journal*, Vol. 13, Jan. 1975, pp. 12–16.

[8]Fuchs, A. J. and Velez, C. E., "In Flight Ground Control of High Drag Satellites Utilizing on-Board Accelerometer Data and Rapid Orbit Prediction Techniques," AIAA Preprint, 74-809, Aug. 1974.

[9]Santora, F. A., "Satellite Drag Perturbations in an Oblate Diurnal Atmosphere," *AIAA Journal,* Sept. 1975, pp. 1212–1216.

[10]Cook, G. E., and King-Hele, D. G., "The Contraction of Satellite Orbits under the Influence of Air Drag, Part V: With Day-to-Night Variation in Air Density," *Philosophical Transactions of the Royal Society,* Vol. 259, 1965.

[11]Kozai, Y., "The Gravitational Field of the Earth Derived from Motions of Three Satellites," *Astronomical Journal,* Vol. 66, 1961, pp. 8–10.

[12]Kozai, Y., "Note on the Motion of a Close Earth Satellite with Small Eccentricity," *Astronomical Journal*, Vol. 64, 1959, pp. 367–377.

[13]King-Hele, D. G., and Cook, G. E., and Scott, D. "The Odd Zonal Harmonics in the Earth's Gravitational Potential," *Planetary and Space Science,* Vol. 13, 1965, pp. 1213–1232.

[14]"Models of Earth's Atmosphere," Superintendent of Documents, U. S. Government Printing Office, NASA SP-8021, 1969.